Applied Surface Science 630 (2023) 157226

Contents lists available at ScienceDirect

Applied Surface Science

journal homepage: www.elsevier.com/locate/apsusc

Full Length Article

Engineering epitaxy and condensation: Fabrication of Ge nanolayers, mechanism and applications

Mohamed Bouabdellaoui [a], Monica Bollani [b], Marco Salvalaglio [c,d], Elie Assaf [a,1], Luc Favre [a], Mathieu Abel [a], Antoine Ronda [a], Olivier Gourhant [e], Fabien Deprat [e], Christophe Duluard [e], Anne-Flore Mallet [a,e], Philippe Vennegues [f], Jean-Noël Aqua [g], Isabelle Berbezier [a,*]

[a] CNRS, IM2NP, Aix-Marseille University, Faculté des Sciences de Saint-Jérôme, case 142, 13397 Marseille, France
[b] Institute of Photonic and Nanotechnology - Consiglio Nazionale delle Ricerche (IFN-CNR), L-NESS, via Anzani 42, Como, Italy
[c] TU-Dresden, Institute of Scientific Computing, Dresden, Germany
[d] Dresden Center for Computational Materials Science, Dresden, Germany
[e] Digital Front End Manufacturing & Technology STMicroelectronics Crolles, France
[f] CNRS, Université Côte d'Azur, CRHEA, Rue Bernard Gregory, 06560 Valbonne, France
[g] CNRS, INSP, Sorbonne University, Paris, France

ARTICLE INFO

Keywords:
Epitaxy
Condensation
Strain relaxation
Morphological evolution
Nanopatterning
Ge photodiodes

ABSTRACT

Superior properties for complex photonic integrated circuits can be obtained by materials other than silicon but compatible with established silicon electronics, e.g., germanium. In this work, we demonstrate the integration with silicon of fully relaxed germanium-on-insulator nanolayers enabled by micro-holes patterning. The heterosystems are fabricated thanks to the combination of epitaxy, electron beam lithography, and condensation. High resolution transmission electron microscopy and geometrical phase analyses show that for holes patterning with periodicities lower than 1 μm, the germanium nanolayers are fully relaxed and free of extended defects, while having numerous defects for larger periodicities and unpatterned settings. The experimental results are discussed with the aid of calculations of the stress for coherent epitaxial silicon–germanium layer with finite size effects and phase-field simulations accounting for the morphological evolution of the germanium crystals. The fabrication method presented here enables the growth of thick monocrystalline germanium-on-insulator layers, with great potential for optoelectronic devices with tunable dimensions and high quality. Also, these systems are suitable for high-speed germanium-on-Si photodetectors with enhanced quantum efficiency resulting from light manipulation by the array of holes. This innovative system, which is expected to operate at the visible and near-infrared range of wavelengths, has huge potential for cutting-edge applications where photodetectors and bipolar transistors are integrated into the same wafer e.g. facial recognition and LIDAR.

1. Introduction

The silicon (Si) photonic platform is the mainstream system used currently in optoelectronics due to its scalability up to 12 in. wafers and wafer-scale co-integration with high-speed electronics using existing techniques [1,2,3,4]. However, its interest goes far beyond optical communications at the 1.55 μm wavelength used by fiber optic telecommunication systems [5,6]. For instance, for applications such as 3D imaging, facial recognition, and LIDAR (Laser Imaging, Detection, and Ranging), it becomes necessary for the sensor to operate in the near-infrared (NIR) wavelength range, particularly at 940 nm, which is crucial for daylight applications [7,8,9,10,11]. In parallel, the sensor, which must detect this light, must be inexpensive for large consumer applications (i.e., smartphones or vehicle driver assistance systems); this implies using cheap materials and the smallest possible sensor size (pixel size<10 μm). It should be used at 25 °C (uncooled technology) in all-weather conditions (typically at 940 nm or 1150 nm, which correspond to the minimum absorption in the atmosphere spectrum). It should be reliable and capable of capturing temporally registered and calibrated data for high dimensionality angle (360°) with a fast update

* Corresponding author.
E-mail address: isabelle.berbezier@im2np.fr (I. Berbezier).
[1] Present address: XFAB, Corbeil Essone, France.

https://doi.org/10.1016/j.apsusc.2023.157226
Received 18 January 2023; Received in revised form 4 April 2023; Accepted 6 April 2023
Available online 18 April 2023

rate and sub-ms response time. Quantum Efficiency (QE) strongly influences the performances of the image sensor (i.e. signal-to-noise ratio and consumption). For wavelengths between 900 and 1100 nm, Si has a much lower QE than germanium (Ge). for instance, at 940 nm, the absorption coefficient of Ge is more than orders of magnitude higher than Si [12]. Ge-based thin films have also higher electron and hole mobilities compared to Si, which can be further increased through strain engineering [13,14,15,16,17,18,19,20,21,22], to improve the photodetector performances. However, even if the strained Ge film (i.e., Ge-on-Si or Ge-on-SOI films) can improve the absorption coefficient at long wavelengths [23], they do not allow for overcoming the speed limitation. Most importantly, excessive stress in the film leads to large wafer bowing and significant densities of extended defects that act as centers of recombination of the electron-hole pairs formed during light absorption.

The most significant bottleneck for the fabrication of a Ge-based photodetector is that the growth of monocrystalline Ge layers integrated on Si(001) substrate results strained due to the 4.2 % lattice mismatch and eventually leads to a large density of dislocations [24,25]. Various methods to lower this density (to $\sim 10^6/cm^2$) in Ge have been suggested and attested by the fabrication of high-performance NIR devices, often comparable to systems integrating III-V heterostructures [26]. The epitaxial growth of thick layers of pure Ge on Si has been successfully achieved using Sb surfactant-assisted epitaxy [27]. In this process, Sb induces a transition in strain relaxation at a critical composition $\sim x = 0.6$ above which full relaxation is achieved by a network of full edge dislocation confined to the interface. 100 nm thick $Si_{1-x}Ge_x$ films ($x < 0.3$) with surface roughness values about 1 nm and abrupt interfaces has been obtained [28]. The reduction of dislocations is also commonly achieved by a two-step process involving first the growth of virtual substrates composed of SiGe buffer layers either compositionally graded [29,30,31,32] or reverse linear graded (RLG) [33] and second the growth of SiGe on top of the buffer layer (i.e. Si (001)/Ge/RLG/$Si_{0.22}Ge_{0.78}$ buffer of 2.4 μm total thickness). However, the large thickness of the buffer layer and the buried Ge layer induce wafer bowing and cracking due to the mismatch of Ge and Si thermal expansion coefficients [34].

Some groups have then tried to decrease the thickness of the complete active structures using ultra-thin $Si_{0.5}Ge_{0.5}$ buffer layers [35,36]. Dislocation-free SiGe structures have also been obtained thanks to 3D heteroepitaxy combined with Ge-concentration gradients [37,38], which avoid both wafer bowing and plastic relaxation. Still, this approach requires deeply patterned substrates, peculiar growth techniques, and considerable buffer layer thickness to reach high Ge content.

New templates have been developed based on Si-on-Nothing (SiON) and Ge-on-Nothing (GeON) platforms. In these systems, the buffer layers are obtained from the reorganization of macro-porous Si and Ge, respectively, fabricated on regular Si substrates using conventional lithography, dry-etching, and annealing routines [39,40,41]. Using a tensely pre-strained substrate has also proven to be an efficient way to inhibit both the formation of islands and the nucleation of misfit dislocations during the growth of Ge-rich SiGe layers. These inhibitions have been observed during the heteroepitaxy of SiGe on pre-strained porous Si [42].

With the recent use of standard Silicon On Insulator (SOI) substrates commonly used for microelectronic devices, new difficulties have arisen in the fabrication of defect-free Ge epitaxial layers. Such layers, whose thickness should be >1 μm for efficient absorption requirements, cannot be fabricated by direct epitaxy. To obtain Ge On Insulator (GeOI) or at least Ge-rich SGOI layers, an attractive method is the condensation technique where a layer of SiGe with low Ge content (typically around 10–20 %) is epitaxially grown on SOI and then thermally oxidized [43,44,45,46,47]. During the oxidation, under appropriate conditions, Si atoms are preferably oxidized, while the Ge atoms are repelled to the $SiO_2/Si_{1-x}Ge_x$ interface resulting in a thin $Si_{1-y}Ge_y$ layer with a higher Ge content at this interface [48,49]. The resulting $Si_{1-y}Ge_y$ layers are embedded between the growing and buried (BOX) oxide layers which act as diffusion barriers against Si and Ge diffusion [50].

Using condensation, Tezuka et al. [51] have obtained an ultrathin (9 nm) SGOI partially relaxed layer with a Ge fraction of 0.56 without introducing a significant dislocation density [52].

However, the growth of a thick Ge layer, which requires the full relaxation of the SGOI layers and the high Ge enrichment of the SGOI layer (Ge concentration > 0,5), without any dislocation, has yet to be reached [53]. It has been reported that mesa isolation can improve the SiGe relaxation during the Ge condensation process [54,48]. Using this technique, it has been shown that a complete relaxation of thin SGOI mesa structures without dislocations is obtained for Ge concentration lower than 0.35 [55,56]. It was also reported that strain could be released by an anomalous swelling relaxation process leading to the undulation of the Ge-rich layer [43,50].

In this study, we give new insights into the fabrication of fully relaxed Ge-based nanolayers for photodetector applications using the combination of SiGe epitaxy, e-beam lithography (EBL), and condensation (selective thermal oxidation). Such monocrystalline Ge-on-insulator layers featuring micro-holes are fully adapted to high-speed Ge-on-Si photodiodes with improved efficiency up to 1700 nm. They can be exploited for many applications, including facial recognition and LIDAR applications [57,58].

2. Experiments

The initial silicon on insulator (SOI) samples were fabricated at STMicroelectronics under standard conditions in a state-of-the-art 300 mm technology semiconductor facility using SOI wafers (001) orientation. The substrates are first thinned by thermal oxidation at 860 °C followed by HF etching to get a SOI thickness of about 14 nm. Prior to oxidation, in-situ cleaning by Siconi is performed to ensure a SOI surface without SiO_2 residual [59].

A schematic representation of the complete process is given in Fig. 1. The condensation process involves: 1) epitaxy of $Si_{1-x}Ge_x$, 2) rapid thermal oxidation, 3) SiO_2 chemical etching, and 4) re-epitaxy of Ge (Fig. 1a). In this study, after the epitaxy of $Si_{1-x}Ge_x$, e-beam lithography is used to create a network of holes and mesas (Fig. 1b). Pure Ge nanolayers, 4 nm thick, embedded between two layers of SiO_2 are obtained at the end of the oxidation process.

The SOI samples are prepared for epitaxy using ex-situ and in-situ cleaning. During ex-situ cleaning, the Si follows a modified Shiraki recipe [60]: (i) 10 min in HNO_3 (65 %) heated at 70 °C, (ii) 1 min in deionized water, and (iii) 30 s in HF (5 %). The samples are then cleaned and annealed in an ultra-high vacuum MBE growth chamber (RIBER SIVA 32, 2 in. growth chamber) with a base pressure of $\sim 10^{-10}$ torr at

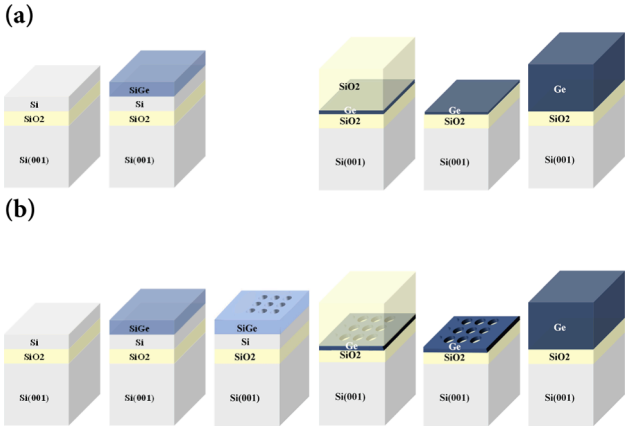

Fig. 1. Schematic representation of the chronological steps of the process: (a) on full scale wafer; (b) when including the EBL patterning steps.

550 °C for 30 min. After in situ cleaning, the $Si_{1-x}Ge_x$ layers with x = 0.2 are deposited at 450 °C using effusion source and electron beam evaporator for Ge and Si, respectively. At this stage, the samples consist of 20 nm thick $Si_{0.8}Ge_{0.2}$ epitaxial layer on 14 nm (0 0 1)Si on 20 nm SiO_2 on (0 0 1)Si substrate (SGOI).Circular holes are realized by electron-beam lithography (EBL) on the upper surface of the $Si_{0.8}Ge_{0.2}$ thin film after cleaning by an ultrasonic treatment with organic solvents. During EBL, different doses have been used to create the holes with diameters of 100–150 nm and periodicities varying between 0.5 and 1.50 μm. The Poly(methyl methacrylate) PMMA resist is spin coated on the substrate and is baked successively on a hot plate at 160 °C for 5 min. The acceleration voltage of 30 kV and an applied dose between 300 and 310μC/cm2 were used to write the patterns on the resist directly. After exposure, PMMA is developed in a solution of methyl isobutyl ketone (MIBK) and isopropanol (IPA) in a 1:3 ratio; MIBK dilution will practically increase the contrast to have a well-defined profile of patterns. The sample is agitated gently during the development for 90 s and, afterwards, it is transferred in IPA as a stopper for 60 s and then is dried by blowing the pure nitrogen. In the next step, the pattern is transferred to the substrate by reactive ion etching (RIE) in a CF_4 plasma, using 50 W of radio frequency power and a total gas pressure of 5.4mTorr. Finally, the resist is removed using acetone, and the sample surface is exposed to O_2 plasma to remove any residual resist. After EBL patterning, low-temperature oxidation of the sample was carried out at 750 °C for 7 h by steps of 30 min using a Rapid Thermal Oxidation (RTO) furnace JIPELEC (JetFirst300). The equipment is dedicated uniquely to column IV elements oxidation. After oxidation, the upper SiO_2 layer of the samples is dissolved in HF solution (5 %). The etch rate of SiO2 in HF solutions has been first calibrated as a function of the HF concentration of the solution. The reaction stops at the Si surface and leaves the surface hydrogen passivated.

The morphological evolution of the films is evaluated by scanning electron microscopy (SEM) using a high-resolution ZEISS model Gemini 500. A FEI Titan 80–300 and a Spectra 200 corrected microscopes both operated at 200 kV were used for high-resolution transmission electron microscopy (HR-TEM) observations and for high resolution scanning transmission electron microscopy high angle angular dark field (HR-STEM HAADF) observations respectively. The TEM cross-section samples were prepared using a FEI Helios 600 Dual Beam Ga^+ focus ion beam (FIB). Geometric Phase Analyses (GPA) were performed on HR-TEM images using Digital Micrograph software. They give a local quantitative determination of the lattice deformation in the condensed layer. All the TEM images presented here are cross-section along the Si [1 1 0] axis.

3. Results

An overview of the overall process was given in the experimental part. But the oxidation process is more complex and includes different steps which will be detailed below. The condensation of the Ge layer proceeds by the selective oxidation during RTO of the Si atoms in a SiGe layer. At low temperature (<800 °C), four different stages of oxidation can be distinguished (Fig. 2). The initial samples consist of $Si_{1-x}Ge_x/Si/SiO_2/$(0 0 1)Si (SG-SOI) with standard $Si_{1-x}Ge_x$ composition (x = 0.2) and thickness (h = 20 nm) (Fig. 2a). A cross-section of the initial SG-SOI sample where the uniformity of the thickness of the stacked layers can be well appreciated, is given Fig. 3a. The image confirms the absence of extended defects as is commonly observed for such conventional samples [61].

The first step is the oxidation of the $Si_{0.8}Ge_{0.2}$ epitaxial layer which leads to the growth of a Ge rich layer on top of the $Si_{0.8}Ge_{0.2}$ layer. During this step and before the oxidation of the underlying SOI layer, the samples consist of $Si_{1-y}Ge_y/Si_{0.8}Ge_{0.2}$ stacked epitaxial layers on SOI (Fig. 2b), capped by a SiO_2 layer on top. The EDX [44] analyses have shown that the newly formed $Si_{1-y}Ge_y$ layer has a concentrations y = 0.5, while the concentration of the underneath $Si_{0.8}Ge_{0.2}$ layer remains

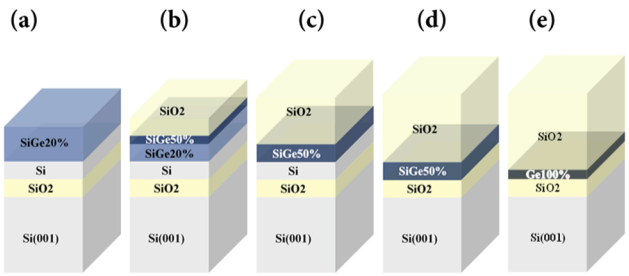

Fig. 2. Schematic representation of the successive condensation steps during rapid thermal oxidation (RTO) at 750 °C: (a) initial sample with the SiGe (x = 0.2, h = 20 nm) epitaxial layer on top of SOI; progressive transformation of the $Si_{0.2}Ge_{0.2}$ into $Si_{0.5}Ge_{0.5}$ results into (b) $SiO_2/Si_{0.5}Ge_{0.5}/Si_{0.2}Ge_{0.2}/Si/SiO_2$ and (c) $SiO_2/Si_{0.5}Ge_{0.5}/Si/SiO_2$ stacked layers; (d) oxidation of the SOI layer until the system reduces to $SiO_2/Si_{0.5}Ge_{0.5}/SiO_2$; (e) oxidation of the Si atoms present in the $Si_{0.5}Ge_{0.5}$ until the obtention of pure Ge/ SiO_2.

unchanged (Fig. 3b). The $Si_{0.5}Ge_{0.5}$ / $Si_{0.8}Ge_{0.2}$ layers are epitaxially strained to the SOI substrate without extended defects as already demonstrated in [44]. It was shown by GPA that the lattice parameters of $Si_{0.5}Ge_{0.5}$ and $Si_{0.8}Ge_{0.2}$ planes perpendicular to the surface fitted to the one of the Si substrate ($a_x^{SiGe50\%} = a_x^{SiGe20\%} = a_x^{Si}$), while the lattice parameter of the planes parallel to the surface are much larger than the Si one ($a_y^{SiGe50\%} > a_y^{SiGe20\%} > a_y^{Si}$)[44]. This fully elastic tetragonal distortion is in good agreement with the expected deformation at the respective concentrations ($\Delta a_y^{SiGe50\%} = 3.41\%; \Delta a_y^{SiGe20\%} = 1.33\%$). At the end of this step, the $Si_{0.8}Ge_{0.2}$ is totally oxidized and has been replaced by a single Ge-rich $Si_{0.5}Ge_{0.5}$ layer epitaxially grown on the SOI layer (Fig. 2c). The $Si_{0.5}Ge_{0.5}$/SOI stacked layers are well visible on the TEM cross-section image (Fig. 3c). The GPA analysis of the HRTEM image (Fig. 4a-I) shows that the $Si_{0.5}Ge_{0.5}$ layer is still strained to the SOI, with a tetragonal distortion analogous to the layer with same composition in the preceding multilayer configuration ($\Delta a_y^{SiGe50\%} = 3.41\%$, $a_x^{SiGe50\%} = a_x^{Si}$, Fig. 4a).

During this oxidation step, when oxygen starts to oxidize the Si atoms of the $Si_{0.5}Ge_{0.5}$ layer, the excess of Ge atoms at the top of the $Si_{0.5}Ge_{0.5}$ layer move through the $Si_{0.5}Ge_{0.5}$ film, while they are stopped at the $Si_{0.5}Ge_{0.5}$/Si interface. Indeed, the diffusion coefficient of Ge in $Si_{0.5}Ge_{0.5}$ is 5 orders of magnitude higher than in Si at the oxidation temperature. The Ge atoms then diffuse through the $Si_{0.5}Ge_{0.5}$ layer up to the $Si_{0.5}Ge_{0.5}$/Si bottom interface. At this interface, because there is almost no diffusion of Ge in Si, the Ge in excess is expelled from the $Si_{0.5}Ge_{0.5}$ layer, following a rapid local exchange mechanism between Ge and Si, similar to a two-layer segregation mechanism. Such a situation allows to keep the 50 % composition which corresponds to the minimum entropy term of the $Si_{0.5}Ge_{0.5}$ alloy [44]. In this two-layer system, the combination of kinetic frustration and local minimum of energy guarantee the stabilization of 50 % composition.

The second step of condensation, is the oxidation of the silicon-on insulator layer. During this stage, the $Si_{0.5}Ge_{0.5}$ layer remains unchanged (thickness and concentration), while the Si atoms of the SOI layer are oxidized. The thickness of this layer decreases linearly with oxidation time (while the thickness of the oxide top layer increases linearly). At the end of this oxidation step, the SOI layer has been fully oxidized (and transformed into SiO_2) with an effective shift downward of the $Si_{0.5}Ge_{0.5}$ layer. A stacking of $SiO_2/Si_{0.5}Ge_{0.5}/SiO_2/$(0 0 1)Si is obtained (Fig. 2d). The $Si_{0.5}Ge_{0.5}$ layer is perfectly flat and free of defects (Fig. 3d) and is still strained with again the same tetragonal distortion of the crystalline cell as it had when the SOI underneath layer was present (and even if this layer is no longer present underneath to maintain epitaxial relationship) (Fig. 4b). At this condensation stage, following this low temperature condensation process, the strain remains the same as those of SiGe50%/SOI (Fig. 4a).

The third step of condensation is the selective oxidation of the

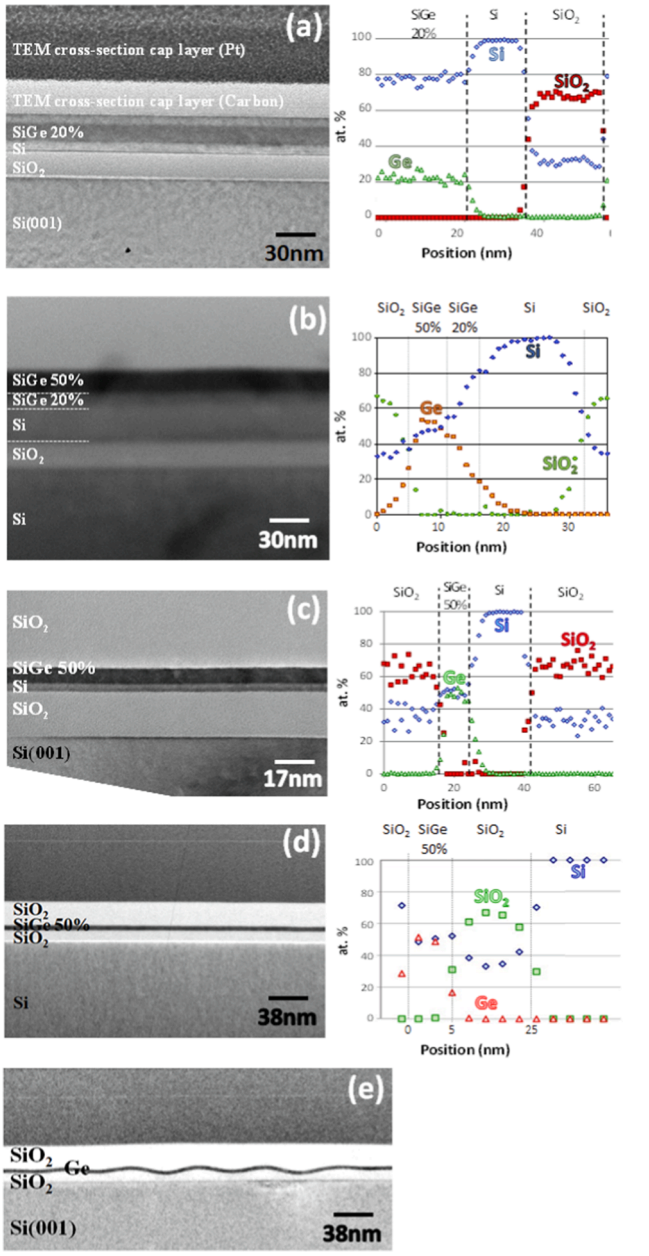

Fig. 3. left column: TEM cross-section images of the samples at increasing times of condensation (a) SiGe20%/SOI; (b) SiGe50%/SiGe20%/SOI; (c) SiGe50%/SOI; (d) SiGe50%/SiO2; (e) SiO2/Ge100%/SiO2; right column: EDX profile analyses of the (a-d) samples.

$Si_{0.5}Ge_{0.5}$ layer. It is important to notice, that the quantity of Si atoms available for oxidation decreases very rapidly associated with a very fast enrichment of the $Si_{1-y}Ge_y$ layer until 100 % Ge. The first relaxation stages are observed during this condensation step, for $y > 0.5$. Starting from this critical concentration, there is a partial and local relaxation which was revealed by HR-TEM observations. Along the interface, large variations of strain distribution on different areas were quantitatively assessed by GPA, even if the overall relaxation of the layer remains very low owing to its planar geometry. GPA confirmed that the local thickening of the layer leads to the local relaxation of the strain accumulated during condensation of Ge due to the presence of free surfaces deviating from the planar one, namely with nonvanishing normal component along the in-plane direction. The resulting deformation in the sample further demonstrates that SiO_2 can serve as a compliant substrate for strain engineering of defect-free Ge rich $Si_{1-y}Ge_y$ thin films.

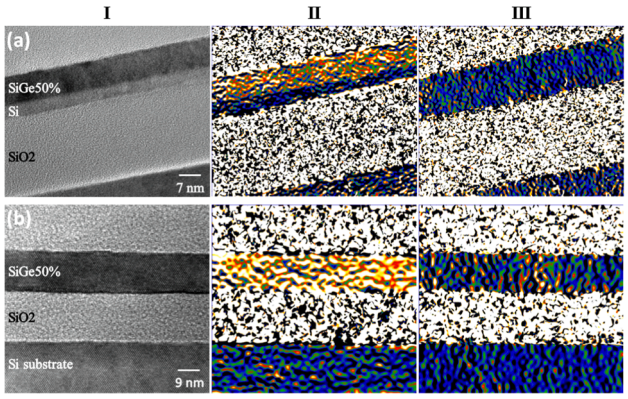

Fig. 4. HRTEM (I) and GPA (II and III correspond to $\varepsilon_{yy}^{SiGe50\%}$ and $\varepsilon_{xx}^{SiGe50\%}$ respectively): (a) SiGe50%/SOI and (b) SiGe50%/Si(001) samples. The same color code is used for the two samples.

At Ge concentrations approaching pure Ge, however, the layer exhibits dislocations and large periodic undulations following a buckling instability phenomenon associated to the swelling of the Ge layer into the oxide. An example of such undulations is given on the TEM cross-section image of Fig. 3e. The very large strain variations, together with the motion of the Ge layer during observation (under the electron beam), have prevented a detailed characterization of the strain field in these layers.

In a second series of experiments, 10x10 μm^2 arrays of holes dedicated to photon trapping, with 100 to 150 nm diameters and different periodicities between 0,5 and 1,5μm were drawn by EBL on the top of the $Si_{1-x}Ge_x$ layer (Figure S1). The purpose of the arrays of holes is twofold: first, to create resonant cavities to enhance Ge PDs external QE and speed, and second, to allow for an additional relaxation of the strain introducing lateral surfaces. The holes have very narrow depths, lower than the thickness of the epitaxial $Si_{1-x}Ge_x$ layer to avoid the lateral oxidation and enlargement of the holes. The samples are then oxidized at low temperature following the same protocol to that used in the first series of experiments (described above). The morphologies of the three typical layers with holes periodicities of 0.7, 1 and 1.5 μm were examined by SEM after SiO_2 oxide etching. Both the unpatterned film (Fig. 5a) and the areas patterned with large periodicities (1 μm and 1.5 μm) (Fig. 5c and 5d, respectively) evidence the presence of a cross-hatch pattern representative of threading dislocations commonly associated to a large density of misfit dislocations which is expected to plastically relax the strain as already previously observed [62].

In contrast, on the patterned area with 0.7 μm periodicity (Fig. 5b),

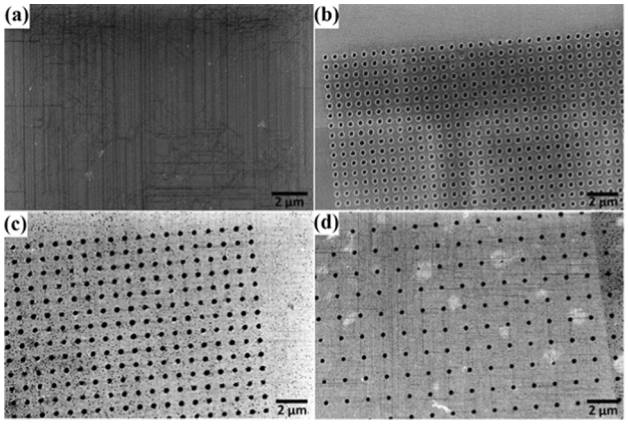

Fig. 5. SEM observations of the samples surface after condensation and SiO_2 etching: (a) unpatterned area; (b), (c) and (d) patterned areas with holes periodicity of 0.7, 1 and 1.5 μm respectively.

there is no evidence of dislocations (the dark trails correspond only to image artifacts). The high-resolution STEM HAADF image of the middle of a pattern confirms the absence of dislocation in the film (Fig. 6d). This evidence suggests that, for periodicity below a critical length, the nucleation of dislocations is inhibited.

The aspects to focus on are now the assessment of the mechanisms at play and to determine whether for relatively small periodicities of patterned holes, the pure Ge nanolayer is relaxed. The large-scale cross-section TEM images of the sample exhibit a ~ 4 nm homogeneous thick layer (Figure S2). EDX scan depth profile of a mesa evidences a concentration of around 100 % Ge in the nanolayer (Fig. 6c). A slight decrease of the concentration is observed on the edge of the mesa at the two Ge/SiO2 interfaces. Considering the nm-size extension of this spreading, it most likely comes from the integration at the border of the two materials in the EDX analysis (because of the diameter of the electron beam). STEM-HAADF images of the patterned areas show that the initial shallow holes, have expanded during the oxidation both laterally (due to lateral oxidation) and in depth through the top SiO_2 layer, until reaching the Ge layer (Fig. 6b) which has broken up at the pattern's location (Fig. 6b). The 700 nm wide Ge mesas formed exhibit rounded and thicker areas at each end (further discussions on morphologies are reported below).

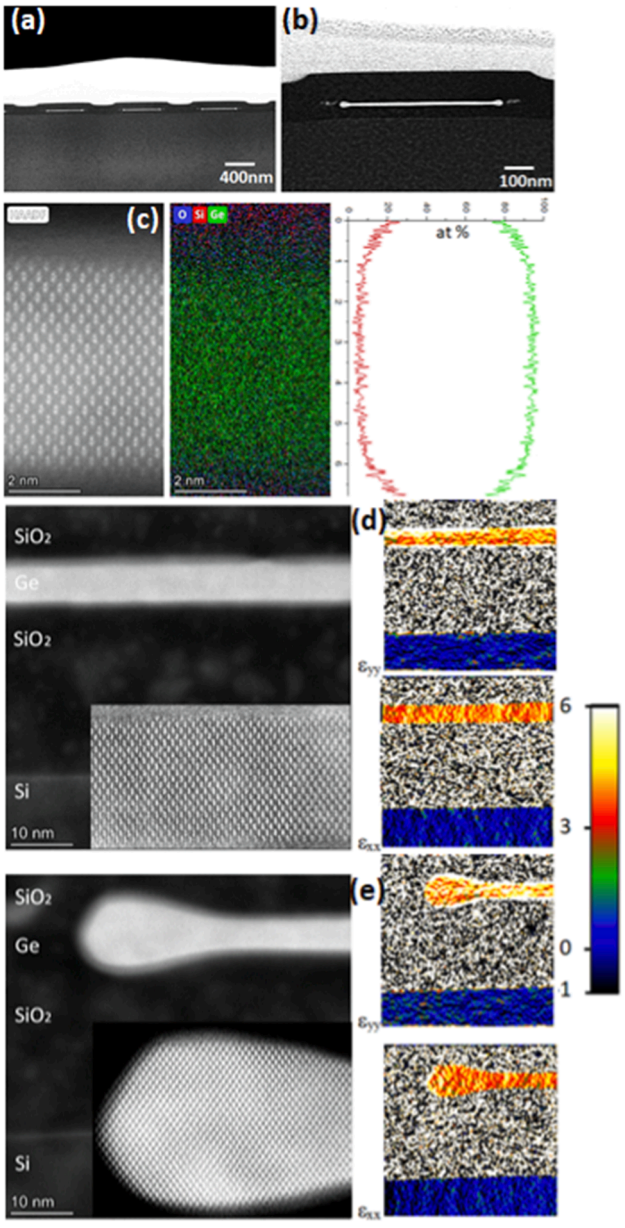

Fig. 6. (a) large scale STEM-HAADF images of the patterned Ge nanolayers obtained for a hole periodicity of 1 μm and (b) zoom of one mesa; (c) from left to right, HR-STEM-HAADF of the Ge nanolayer and corresponding EDX cartography and EDX profile; (d) and (e) left: HR-STEM-HAADF and right: GPA along in plane and out of plane directions; (d)corresponds the middle of a mesa and (e) to the edge.

Fig. 6d-e exemplify the typical STEM images and corresponding GPA strain maps in the left and right columns respectively. The color code of the GPA images and the integration of the deformation along the in-plane × axis ε_{xx} (direction parallel to the sample surface) and out-of-plane y axis ε_{yy} (perpendicular to the sample surface) are reported in Figure S4. The reference chosen for the GPA analyses is the Si substrate. GPA measurements were performed on all the patterns of the same sample in the middle of the pattern and on their edges, to get an accurate assessment of strain. It is noticeable that the strain is almost constant in all the images and in the × and y direction comparing to the Si substrate. One can notice an equal increase of the Ge lattice parameter in the two directions (x and y) of about 4 % as compared that of Si. This corresponds exactly to the mismatch between Si and Ge crystalline cells. Therefore, it shows that the Ge film is perfectly relaxed in the two in-plane directions, without any dislocation.

In order to better understand the mechanisms underlying the relaxation and material redistribution, we analysed simulations of the morphological evolution of an epitaxial film on top of a mesa. We considered a dynamical continuum description of the film evolution ruled by surface diffusion induced by elasticity and capillarity, (see [63] for more details). The simulation of the evolution of a full scale SiGe film on SiO_2 was reported previously [64]. To discuss the interplay among elasticity and the geometry of the Ge crystalline domain under investigation, we can consider first a prototypical system with 1D patterns of width w = 1 μm and infinite in the other direction, consisting of

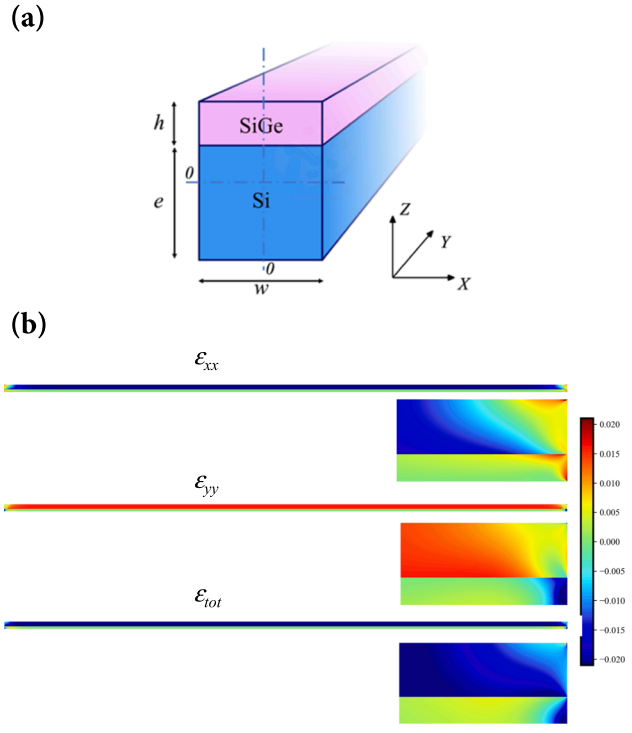

Fig. 7. (a) Schematic of the mesa system under consideration. A film of thickness h is coherently deposited on a mesa of thickness e and width w; (b) Lateral strain maps for a pattern with e/w = 0.01 and h/e = 2. ε_{xx}(up), ε_{yy} (middle) and the total strain (ε_{tot}) are displayed in real proportions and a zoom of the relaxation at the extremity of the mesa is also given in insert.

$Si_{0.5}Ge_{0.5}$ in epitaxy with a thin membrane of Si with respective thicknesses h and e for $Si_{0.5}Ge_{0.5}$ and Si, respectively (Fig. 7a). This mimics the ideal epitaxy of a SiGe layer with a substrate underneath having the lattice spacing of bulk Si. In general, mass transfer occurs mainly at the relaxed areas at the end of the nanolayers in qualitative agreement with the material accumulation observed in Fig. 6. The morphological dynamics is enforced by surface-diffusion that is dictated by gradients in the elastic and surface chemical potential in a classic continuum thermodynamic description [65]. In this two-dimensional-like geometry, elasticity may be solved exactly thanks to the Airy formalism, and the dynamical surface diffusion equation can be solved with a decomposition on eigenmodes, (see [66] and details therein). This analysis reveals different developments depending upon the mesa geometric parameters and finite-size effects. We find that the amplitude and speed of the evolution are controlled by the aspect-ratio of the structures, as well as its absolute scale. More generally we find that the typical zone where elastic relaxation occurs naturally increases when the film height (h) increases. It also increases with the mesa aspect ratio e/w as finite size effects increase. In the considered experimental conditions, the finite size effects are are characterized by a small aspect ratio $e/w < 0.01$ as the geometries correspond de-facto to a film-like configuration. Full relaxation at the top of the SiGe layer could occur when the thickness of the epitaxial film (h) is of the same order or larger than the thickness of the Si membrane ($h/e > 1$) [63], well beyond the aspect-ratio of the structures under investigation. We calculated the morphological evolution in different conditions and we found that a strong relaxation for $Si_{0.5}Ge_{0.5}h = 8$ nm thick and Si membrane with $e = 4$ nm. In these conditions the results show a very limited lateral extension of the relaxation (Fig. 7b) and the film is nearly fully strained.

The same has to be expected in case of strong bonding to the oxide film (pinned interface) being in epitaxy with the Si layer underneath. The relaxation observed experimentally then deviates significantly from the one achieved in epitaxial SiGe/SOI (and Ge/SiO_2). This suggests that an enhanced elastic relaxation occurs, which may be ascribed to the weak Ge/SiO_2 bonding [67,45] accommodating the in-plane lattice parameter of Ge. This is expected to be triggered when lateral free surfaces are introduced in a film-like configuration, and experiments show that this is obtained under a certain periodicity. This can be qualitatively explained as follows. In an unpatterned, ideally-flat 2D strained layer, there would be no in-plane strain release even with free surfaces on top and bottom (i.e., for a suspended, infinitely extended 2D membrane). When introducing patterning, the scenario changes. By focusing on a layer cross-section only, introducing patterning consists of having additional vertical free surfaces which allow for full strain release. Namely, the layer is free to expand in every direction. This, however, may occur if the layer is not pinned on a substrate (Fig. 7) or is expected to occur up to a certain spacing between the additional, vertical free surfaces for a weekly pinned layer. While involving a biaxially strained and holes-patterning, the behavior observed in the experiment may be ascribed to an intermediate configuration among being fully free to relax and fully pinned as in conventional epitaxy.

Further assessing this picture, the morphologies obtained close to the holes introduced patterning closely resemble the ones obtained by diffusion at free surfaces in crystalline systems, namely the motion of the surface driven by the Laplacian of the chemical potential accounting for curvature and anisotropic interface/surface energy densities [68,69]. In Fig. 8, the evolution according to such dynamics is shown and compared to a representative shape from the experiments. In particular, the result of a two-dimensional continuum simulation of interface diffusion with anisotropic interface energy is reported. The simulation is obtained by using a suitable phase-field (PF) model. In brief, the initial condition for the simulation (Fig. 8) corresponds to a rectangular shape for a region with an order parameter, $\varphi = 1$ in the Ge phase surrounded by a region with phase field $\varphi = 0$ outside, with a smooth transition in between (obtained through a function of the hyperbolic tangent of the signed distance from the $\varphi = 0.5$, as in classical phase field models). $\varphi \sim 0.5$ is

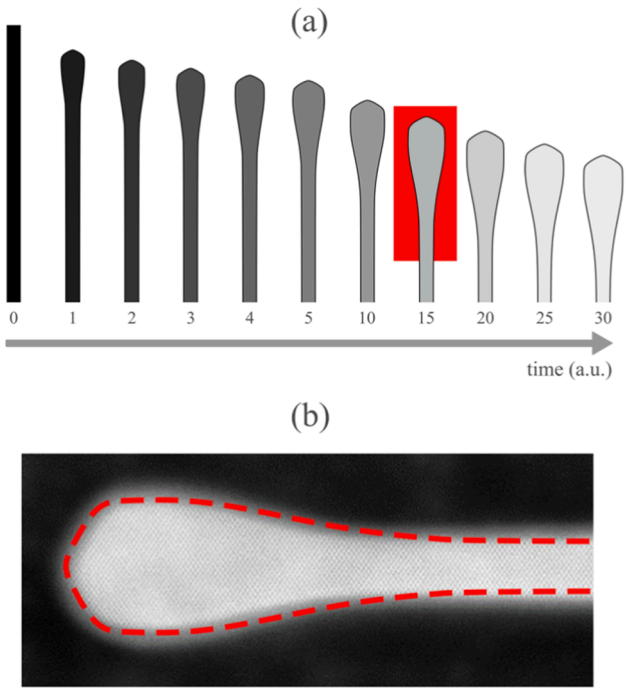

Fig. 8. Insights on the morphological evolution with a PF simulation. (a) Evolution by anisotropic surface/interface diffusion (Laplacian of the chemical potential) for a rectangular domain with an aspect ratio of 0.02 (half of the domain is shown in the figure). Time is expressed in arbitrary units. Simulation parameter referring to notations as in Ref [69]are : $\gamma_0 = 1$, $\beta = 0.05$, $\alpha_i = 0.1$, $\mathbf{m}_i = [\sin(6\theta_i), \cos(6\theta_i)]$, $\theta_i = i\pi/3$ with $i = 0, \cdots, 5$. (b) Comparisons of a representative shape during the evolution obtained by PF simulation ($t = 15$ in panel (a), red dashed line) with the experimental HR-STEM-HAADF of the Ge nanolayer from Fig. 6(a). The area shown in panel (b) corresponds to the red rectangle in panel (a).

identified as the interface among Ge and the surrounding SiO_2. The dynamic is evaluated via the so-called degenerate Cahn-Hilliard equation [70]. The considered phase field model approximates the evolution of a curve by the motion of the interface among phases by the Laplacian chemical potential that corresponds to the curvature for isotropic surface energy (i.e., the continuum model for surface diffusion) [71] in the limit of small interface thicknesses [72]. Moreover, a formulation accounting for interface-energy anisotropy is considered through parametrization of the interface-energy density $\gamma(\hat{\boldsymbol{n}})$, and a regularization for strong-anisotropy regimes is considered. Details of the model and (FEM) [73,74] simulations can be found in Refs. [64,75,76]. $\gamma(\hat{\boldsymbol{n}})$ is set to approximate the main facets of the equilibrium crystal shapes, namely (1 0 0), $(\bar{1}00)$ and {1 1 1} facets. This is achieved by setting minima at orientations every 60°. In Fig. 8(a) the evolution of a rectangular domain is reported. This idealized evolution mimics the shape evolution in a cross-section of the film passing through the holes. It matches almost perfectly the morphology obtained in the experiments assessing a material transport mechanism analogous to a free surface of a crystalline phase, and thus the weak bonding at the Ge/SiO_2 interface discussed above. Fig. 8(b) shows a representative simulation stage (red, dashed line) compared to the experimental morphology from Fig. 6(a). In some sense, the simulations describe a free-standing (in the sense of no additional contributions) interface encoding material transport at the interface in a coarse-grained fashion. However, the same evolution would be observed for either a free-standing crystal (e.g., with shapes as in the grey regions of Fig. 8) or a void with the same shape surrounded by the crystal. With this work, we introduce an element of novelty that Ge surrounded by SiO_2 would evolve similarly to a Ge crystal with free surfaces, analogously to the evolution by diffusion of adatoms thereon. This may be ascribed to the weakly-bonded, amorphous phase, which

behaves *de facto* as a compliant material accommodating any change of shape of the crystalline Ge phase.

It should be noted that the phase field simulations account for capillarity effects only. This is indeed expected to be the major driving force: due to the creation of holes and regions with high curvature (i.e. large surface chemical potential), capillarity dominates. Here, on the one hand, the corrugation of the film is shown to occur without breakups in the absence of patterning but just with the buckling of the thin crystalline layer. On the other hand, with patterning, regions of high curvature are already present and evolve by capillarity only, as also shown by simulations vs experiments comparisons.

Interestingly, in this system dynamics resembling solid-state dewetting is then obtained, but for a crystalline domain embedded in an oxide similarly to a free-standing crystalline domain on a substrate [77,78] *** [79] paving the way for a promising approach to tailor the self-assembly of Ge crystalline nanostructures.

4. Conclusion

In this paper, it is found that the combination of epitaxy, e-beam patterning, and low-temperature condensation produces elastically relaxed and dislocation-free strips of pure Ge films that are promising templates for the regrowth of thick Ge relaxed films. Theoretical simulations of the dynamic evolution of thin films have been exploited to discuss the experimental evidence and shed light on the elastic relaxation and morphological evolution of the layer in the presence of patterns sub-micrometer apart. Growth dynamics was analysed in the prototypical conditions of SiGe/Si coherent epitaxial interface for discussing elasticity effects, representative of epitaxy on a substrate having the lattice spacing of Si in general. For the geometric features realized in the experiments, such an epitaxial system is expected to remain almost fully strained. We conclude that the fully relaxed Ge nanolayers, featuring a flat morphology and free of defects, could only result from an enhanced elastic relaxation possible due to weak Ge/SiO_2 bonds. Such a glissile interface is only obtained when pure Ge is directly in contact with SiO_2, without any Si remaining. Phase field simulations of the morphological evolution obtained in patterned film further assess the weak bonding at the Ge/SiO_2, which behaves de-facto as a free surface for what concerns material transport. The pre-patterning based low-cost process developed here is immediately integrable in the microelectronic industry and paves the path for integrating optically active Ge structures on the Si photonic platform. Moreover, the process can be exploited to obtain the morphological evolutions of Ge crystalline domains with driving forces similar to conventional epitaxial systems but for three-dimensional domains embedded, and de-facto suspended, in oxide. This represents an extremely promising technique for tailoring nanostructures similarly to more conventional epitaxial growth on patterned substrates and solid-state dewetting but for three-dimensional settings rather than for planar arrangements on substrates.

CRediT authorship contribution statement

Mohamed Bouabdellaoui: . **Monica Bollani:** . **Marco Salvalaglio:** Software, Validation, Formal analysis, Data curation. **Elie Assaf:** . **Luc Favre:** . **Mathieu Abel:** . **Antoine Ronda:** . **Olivier Gourhant:** Conceptualization, Visualization, Supervision, Project administration. **Fabien Deprat:** Conceptualization, Visualization, Supervision, Project administration. **Christophe Duluard:** Conceptualization, Visualization, Supervision, Project administration. **Anne-Flore Mallet:** Conceptualization, Visualization, Supervision, Project administration. **Philippe Vennegues:** . **Jean-Noël Aqua:** Software, Validation, Formal analysis, Data curation. **Isabelle Berbezier:** Conceptualization, Formal analysis, Data curation, Writing - review & editing, Supervision, Project administration, Funding acquisition.

Declaration of Competing Interest

The authors declare that they have no known competing financial interests or personal relationships that could have appeared to influence the work reported in this paper.

Data availability

No data was used for the research described in the article.

Appendix A. Supplementary data

Supplementary data to this article can be found online at https://doi.org/10.1016/j.apsusc.2023.157226.

References

[1] A.H. Atabaki, S. Moazeni, F. Pavanello, et al., Integrating photonics with silicon nanoelectronics for next generation of systems on a chip, Nature 556 (2018) 349–354.
[2] G.T. Reed, G. Mashanovich, F.Y. Gardes, D.J. Thomson, Silicon optical modulators, Nat. Photonics 4 (2010) 518–526.
[3] Y. Gao, H. Cansizoglu, K.G. Polat, et al., Photon-trapping microstructures enable high-speed high-efficiency silicon photodiodes, Nat. Photonics 11 (2017) 301–308.
[4] P.C. Eng, S. Song, B. Ping, State-of-the-art photodetectors for optoelectronic integration at telecommunication wavelength, Nanophotonics 4 (2015) 277–301.
[5] J.J. Ackert, D.J. Thomson, L. Shen, et al., High-speed detection at two micrometres with monolithic silicon photodiodes, Nat. Photonics 9 (2015) 393–396.
[6] C.L. Tan, H. Mohseni, Emerging technologies for high performance infrared detectors, Nanophotonics 7 (2017) 169–197.
[7] H. Rong, R. Jones, A. Liu, et al., A continuous-wave Raman silicon laser, Nature 433 (2005) 725–728.
[8] Y. Takahashi, Y. Inui, M. Chihara, T. Asano, R. Terawaki, S. Noda, A micrometre-scale Raman silicon laser with a microwatt threshold, Nature 498 (2013) 470–474.
[9] N.T. Otterstrom, R.O. Behunin, E.A. Kittlaus, Z. Wang, P.T. Rakich, A silicon Brillouin laser, Science 360 (2018) 1113–1116.
[10] B. Unlu, M. Ghasemi, S. Yerci, C. Boztug, Simultaneous crystallization and strain induction enable light-emitting germanium nano/microbridges for infrared lasers, ACS Appl. Nano Mater. 5 (2022) 4700-4709.
[11] S. Lischke, A. Peczek, J.S. Morgan, K. Sun, D. Steckler, Y. Yamamoto, F. Korndörfer, C. Mai, S. Marschmeyer, M. Fraschke, A. Krüger, A. Beling, L. Zimmermann, Ultra-fast germanium photodiode with 3-dB bandwidth of 265 GHz, Nat. Photonics 15 (2021) 925–931.
[12] J. Gosciniak, M.R. Asras, High-bandwidth and high-responsivity waveguide-integrated plasmonic germanium photodetector.
[13] L. Virot, Ultrafast on-chip germanium photodiode, Nat. Photon. 15 (2021) 868–869.
[14] D. Benedikovic, L. Virot, G. Aubin, J.-M. Hartmann, F. Amar, X. Le Roux, C. Alonso-Ramos, É. Cassan, D. Marris-Morini, J.-M. Fédéli, F. Boeuf, B. Szelag, L. Vivien, Silicon–germanium receivers for short-wave-infrared optoelectronics and communications High-speed silicon–germanium receivers, Nanophotonics 10 (2021) 1059–1079.
[15] Y. Shi, D. Zhou, Y. Yu, X. Zhang, 80-GHz germanium waveguide photodiode enabled by parasitic parameter engineering, Photon. Res., **2021**, 9, 605–609; C.G. Littlejohns, M. Nedeljkovic, C.F. Mallinson, et al., Next generation device grade silicon-germanium on insulator, Sci. Rep., 5 (2015) 8288.
[16] L. Virot, D. Benedikovic, B. Szelag, et al., Integrated waveguide PIN photodiodes exploiting lateral Si/Ge/Si heterojunction, Opt. Express 25 (2017) 19487–19496.
[17] C.G. Littlejohns, T. Dominguez Bucio, M. Nedeljkovic, C. Alonso-Ramos, B. Karakus, J.M. Hartmann, X. Le Roux, P. Crozat, E. Cassan, D. Marris-Morini, C. Baudot, F. Boeuf, J.-M. Fédéli, C. Kopp, L. Vivien, Towards a fully functional integrated photonic-electronic platform via a single SiGe growth step, Sci. Rep. 6 (2016) 19425.
[18] M.J. Süess, R. Geiger, R. Minamisawa, G. Schiefler, J. Frigerio, D. Chrastina, G. Isella, R. Spolenak, J. Faist, H. Sigg, Analysis of enhanced light emission from highly strained germanium microbridges, Nat. Photonics 7 (2013) 466–472.
[19] P.M. Mooney, J.O. Chu, SiGe technology: Heteroepitaxy and high-speed microelectronics, Annu. Rev. Mater. Sci. 30 (2000) 335.
[20] A. Dobbie, M. Myronov, R.J.H. Morris, A.H.A. Hassan, M.J. Prest, V.A. Shah, E.H. C. Parker, T.E. Whall, D.R. Leadley, Ultra-high hole mobility exceeding one million in a strained germanium quantum well, Appl. Phys. Lett. 101 (2012), 172108.
[21] Y.S. Li, P. Sookchoo, X. Cui, R. Mohr, D.E. Savage, R.H. Foote, R.B. Jacobson, J. R. Sánchez-Pérez, D.M. Paskiewicz, X. Wu, D.R. Ward, S.N. Coppersmith, M. A. Eriksson, M.G. Lagally, Electronic transport properties of epitaxial Si/SiGe heterostructures grown on single-crystal SiGe nanomembranes, ACS Nano 9 (2015) 4891–4899.
[22] M. Clavel, D. Saladukha, P.S. Goley, T.J. Ochalski, F. Murphy-Armando, R. J. Bodnar, M.K. Hudait, Heterogeneously-grown tunable tensile strained germanium on silicon for photonic devices, ACS Appl. Mater. Interfaces 7 (2015) 26470–26481.

[23] J.-N. Aqua, I. Berbezier, L. Favre, T. Frisch, A. Ronda, Growth and self-organization of SiGe nanostructures, Phys. Rep. 522 (2013) 59–189.
[24] I. Berbezier, A. Ronda, SiGe nanostructures, Surf. Sci. Rep. 64 (2009) 47–98.
[25] D. Marris-Morini, V. Vakarin, J.M. Ramirez, Q. Liu, A. Ballabio, J. Frigerio, M. Montesinos, C. Alonso-Ramos, X. Le Roux, S. Serna, D. Benedikovic, D. Chrastina, L. Vivien, G. Isella, Germanium-based integrated photonics from near- to mid-infrared applications, Nanophotonics 7 (2018) 1781–1793.
[26] A. Portavoce, I. Berbezier, A. Ronda, Sb-surfactant-mediated growth of Si and Ge nanostructures, Phys. Rev. B 69 (2004), 155416.
[27] T.F. Wietler, J. Schmidt, D. Tetzlaff, E. Bugiel, Surfactant-mediated epitaxy of silicon germanium films on silicon (001) substrates, Thin Solid Films 557 (2014) 27–30.
[28] K. Lyutovich, M. Bauer, E. Kasper, H.-J. Herzog, T. Perova, R. Maurice, C. Hofer, C. Teichert, Thin SiGe buffers with high Ge content for n-MOSFETs, Mat. Sci. Eng.: B 89 (2002) 341–345.
[29] B. Gallas, J.M. Hartmann, I. Berbezier, M. Abdallah, J. Zhang, J.J. Harris, B. A. Joyce, Influence of misfit and threading dislocations on the surface morphology of SiGe graded-layers, J. Cryst. Growth 201–202 (1999) 547–550.
[30] I. Berbezier, A. Ronda, A. Portavoce, SiGe nanostructures: new insights into growth processes, J. Phys. Condens. Matter 14 (2002) 8283–8331.
[31] T.S. Yoon, J. Liu, A.M. Noori, M.S. Goorsky, Y.H. Xie, Surface roughness and dislocation distribution in compositionally graded relaxed SiGe buffer layer with inserted-strained Si layers, Appl. Phys. Lett. 87 (2005), 012104.
[32] G. Scappucci, C. Kloeffel, F.A. Zwanenburg, D. Loss, M. Myronov, J.-J. Zhang, S. De Franceschi, G. Katsaros, M. Veldhorst, The germanium quantum information route, Nat. Rev. Mater. 6 (2021) 926–943.
[33] S. Cecchi, E. Gatti, D. Chrastina, J. Frigerio, E.M. Gubler, D.J. Paul, M. Guzzi, G. Isella, Thin SiGe virtual substrates for Ge heterostructures integration on silicon, J. Appl. Phys. 115 (2014), 093502.
[34] J. Nakatsuru, H. Date, S. Mashiro, M. Ikemoto, Growth of high quality Ge epitaxial layer on Si(100) substrate using ultra thin Si0.5Ge0.5 buffer, MRS Proc. 891 (**2005**) 0891-EE07-24.1-6.
[35] H.C. Luan, D.R. Lim, K.K. Lee, K.M. Chen, J.G. Sandland, K. Wada, L.C. Kimerling, High-quality Ge epilayers on Si with low threading-dislocation densities, Appl. Phys. Lett. 75 (1999) 2909–2911.
[36] F. Isa, M. Salvalaglio, Y.A. Rojas Dasilva, M. Meduňa, M. Barget, A. Jung, T. Kreiliger, G. Isella, R. Erni, F. Pezzoli, E. Bonera, P. Niedermann, P. Gröning, F. Montalenti, H. von Känel, Highly mismatched, dislocation-free SiGe/Si heterostructures, Adv. Mater. 28 (2016) 884–888.
[37] F. Montalenti, F. Rovaris, R. Bergamaschini, L. Miglio, M. Salvalaglio, G. Isella, F. Isa, H. Von Känel, Dislocation-free SiGe/Si heterostructures, Crystals 8 (2018) 257–273.
[38] A. Osman, M. Nedeljkovic, J.S. Penades, Y. Wu, Z. Qu, A.Z. Khokhar, K. Debnath, G.Z. Mashanovich, Suspended low-loss germanium waveguides for the longwave infrared Opt. Lett. 43 (2018) 5997–6000.
[39] M. Aouassa, S. Escoubas, A. Ronda, L. Favre, S. Gouder, R. Mahamdi, E. Arbaoui, A. Halimaoui, I. Berbezier, Ultra-thin planar fully relaxed Ge pseudo-substrate on compliant porous silicon template layer, Appl. Phys. Lett. 101 (2012), 233105.
[40] I. Berbezier, J.N. Aqua, M. Aouassa, L. Favre, S. Escoubas, A. Gouyé, A. Ronda, Accommodation of SiGe strain on a universally compliant porous silicon substrate, Phys. Rev. B 90 (2014), 035315.
[41] T. David, J.N. Aqua, K. Liu, L. Favre, A. Ronda, M. Abbarchi, J.-B. Claude, I. Berbezier, New strategies for producing defect free SiGe strained nanolayers, Sci. Rep. 8 (2018) 2891.
[42] T. David, A. Benkouider, J.N. Aqua, M. Cabie, L. Favre, T. Neisius, M. Abbarchi, M. Naffouti, A. Ronda, K. Liu, I. Berbezier, Kinetics and energetics of Ge condensation in SiGe oxidation, J. Phys. Chem. C 119 (2015) 24606–24613.
[43] Y. Kim, M. Yokoyama, N. Taoka, M. Takenaka, S. Takagi, Ge-rich SiGe-on-insulator for waveguide optical modulator application fabricated by Ge condensation and SiGe regrowth, Opt. Express 21 (2013) 19615–19623.
[44] K.W. Jo, W.K. Kim, M. Takenaka, S. Takagi, Impact of SiGe layer thickness in starting substrates on strained Ge-on-insulator pMOSFETs fabricated by Ge condensation method, Appl. Phys. Lett. 114 (2019), 062101.
[45] G. Lin, D. Liang, J. Wang, C. Yu, C. Li, S. Chen, W. Huang, J. Wang, J. Xu, Strain evolution in SiGe-on-insulator fabricated by a modified germanium condensation technique with gradually reduced condensation temperature, Mater. Sci. Semicond. Process. 97 (2019) 56–61.
[46] E. Assaf, I. Berbezier, M. Bouabdellaoui, M. Abbarchi, A. Ronda, D. Valenducq, F. Deprat, O. Gourhant, A. Campos, L. Favre, Local defect-free elastic strain relaxation of Si1-xGex embedded into SiO2, Appl. Surf. Sci. 590 (2022), 153015.
[47] T. David, K. Liu, S. Fernandez, M.-I. Richard, A. Ronda, L. Favre, M. Abbarchi, A. Benkouider, J.-N. Aqua, M. Peters, P. Voorhees, O. Thomas, I. Berbezier, Remarkable strength characteristics of defect-free SiGe/Si heterostructures obtained by Ge condensation, J. Phys. Chem. C 120 (2016) 20333–20340.
[48] L. de los Santos Valladares, A. Bustamante Dominguez, A. Ionescu.
[49] L. de los Santos Valladares, A. Bustamante Dominguez, J. Llandro, S. Holmes, O. Avalos Quispe,, R. Langford, J. Albino Aguiar, C.H.W. Barnes "Surface morphology of amorphous germanium thin films following thermal outgassing of SiO2/Si substrates", Appl. Surf. Sci, 316 (2014) 15-21.
[50] T. David, I. Berbezier, J.N. Aqua, M. Abbarchi, A. Ronda, N. Pons, F. Domart, P. Costaganna, G. Uren, L. Favre, New strategies for engineering tensile strained Si layers for novel n-type MOSFET, ACS Appl. Mater. Interfaces 13 (2021) 1807–1817.
[51] T. Tezuka, N. Sugiyama, S. Takagi, Fabrication of strained Si on an ultrathin SiGe-on-insulator virtual substrate with a high-Ge fraction, Appl. Phys. Lett. 79 (2001) 1798.
[52] S. Reboh, R. Coquand, S. Barraud, N. Loubet, N. Bernier, G. Audoit, J.L. Rouviere, E. Augendre, J. Li, J. Gaudiello, N. Gambacorti, T. Yamashita, O. Faynot, Strain, stress, and mechanical relaxation in fin-patterned Si/SiGe multilayers for sub-7 nm nanosheet gate-all-around device technology, Appl. Phys. Lett. 112 (2018), 051901.
[53] S. Nakaharai, T. Tezuka, N. Hirashita, E. Toyoda, Y, Moriyama, N Sugiyama, S Takagi, "The generation of crystal defects in Ge-on-insulator (GOI) layers in theGe-condensation process" Semicond. Sci. Technol., **2007**, 22, S103–S106.
[54] Yiding Lin, Kwang Hong Lee, Shuyu Bao, Xin Guo, Hong Wang, Jurgen Michel, and Chuan Seng Tan, "High-efficiency normal-incidence vertical p-i-n photodetectors on a germanium-on-insulator platform", Photonics Research, **2017**, 5, 702-709.
[55] T. Tezuka, N. Sugiyama, S.I. Takagi, Dislocation-free relaxed SiGe-on-insulator mesa structures fabricated by high temperature oxidation, J. Appl. Phys. 94 (2003) 7553.
[56] H. Cansizoglu, C. Bartolo-Perez, Y. Gao, E. Ponizovskaya Devine, S. Ghandiparsi, K. G. Polat, H.H. Mamtaz, T. Yamada, A.F. Elrefaie, S.-Y. Wang, M.S. Islam, Surface-illuminated photon-trapping high-speed Ge-on-Si photodiodes with improved efficiency up to 1700 nm, Photonic Research 6 (2018) 734–742.
[57] H. Tran, T. Pham, J. Margetis, Y. Zhou, W. Dou, P.C. Grant, J.M. Grant, S. Al-Kabi, G. Sun, R.A. Soref, et al., Si-based GeSn photodetectors toward mid-infrared imaging applications, ACS Photonics 6 (2019) 2807–2815.
[58] N.H. Ngo, A.Q. Nguyen, F.M. Bufler, Y. Kamakura, H. Mutoh, T. Shimura, et al., Toward the super temporal resolution image sensor with a germanium photodiode for visible light, Sensors 20 (2020) 6895–6911.
[59] J. Tang, N. Ingle, D. Yang, Smooth SiConi etch for silicon-containing films, Patent US8501629B2, Applied Mat. Inc., 2013.
[60] A. Ishizaka, Y. Shiraki, Low temperature surface cleaning of silicon and its application to silicon MBE, J. Electrochem. Soc. 133 (1986) 666.
[61] H. Donglin, J. Ruoyun, Y. Liqiang, J. Jinlong, C. Xiaoqiang, L. Cheng, H. Wei, C. Songyan, K. Shaoying, Dislocation nucleation triggered by thermal stress during Ge/Si wafer bonding process at low annealing temperature, Appl. Surf. Scie. 568 (2021), 150979.
[62] T. David, J.N. Aqua, K. Liu, L. Favre, A. Ronda, M. Abbarchi, J.B. Claude, I. Berbezier, "New strategies for producing defect free SiGe strained nanolayers, Sci. Rep. 8 (2018) 2891.
[63] Kennet D. R. Hannikainen, Luc Favre, Fabien Deprat, Olivier Gourhant, Isabelle Berbezier, Jean-Noël Aqua, Shape relaxation of epitaxial mesa for finite-size strain-engineering, arXiv:2209.08070.
[64] M. Salvalaglio, F. Montalenti, Fine control of plastic and elastic relaxation in Ge/Si vertical heterostructures, J. Appl. Phys. 116 (2014), 104306.
[65] W.W. Mullins, Theory of thermal grooving, J. Appl. Phys. 28 (1957) 333–339.
[66] W.C. Carter, A.R. Roosen, J.W. Cahn, J.E. Taylor, Shape evolution by surface diffusion and surface attachment limited kinetics on completely faceted surfaces, Acta Metall. Mater. 43 (1995) 4309–4323.
[67] C. Dabard, A.A. Shklyaev, V.A. Armbrister, A.L. Aseev, Effect of deposition conditions on the thermal stability of Ge layers on SiO2 and their dewetting behavior, Thin Solid Films 693 (2020), 137681.
[68] M. Salvalaglio, R. Backofen, R. Bergamaschini, F. Montalenti, A. Voigt, Faceting of equilibrium and metastable nanostructures: a phase-field model of surface diffusion tackling realistic shapes, Cryst. Growth Des. 15 (2015) 2787–2794.
[69] B. Li, J. Lowengrub, A. Ratz, A. Voigt, Geometric evolution laws for thin crystalline films: modeling and numerics, Comm. Comput. Phys. 6 (2009) 433.
[70] W. Cahn, J.E. Hilliard, Free energy of a nonuniform system I. Interfacial free energy, J. Chem. Phys. 28 (1958) 258–267.
[71] S. Vey, A. Voigt, AMDiS: adaptive multidimensional simulations, Comput. Vis. Sci. 10 (2007) 57–67.
[72] B. Li, J. Lowengrub, A. Rätz, A. Voigt, Geometric evolution laws for thin crystalline films: modeling and numerics, Comm. Comput. Phys. 6 (2009) 433.
[73] T. Witkowski, S. Ling, S. Praetorius, A. Voigt, Software concepts and numerical algorithms for a scalable adaptive parallel finite element method, Adv. Computat. Math. 41 (2015) 1145–1177.
[74] M. Salvalaglio, M. Selch, A. Voigt, S. Wise, Doubly degenerate diffuse interface models of anisotropic surface diffusion, Math. Method Appl. Sci. 44 (2021) 5406.
[75] S. Torabi, J. Lowengrub, A. Voigt, S. Wise, A new phase-field model for strongly anisotropic systems. Proc. Roy. Soc. A: Math. Phys. Eng. Sci. 465 (2009) 1337-1359.
[76] C.V. Thompson, Solid-state dewetting of thin films, Annu. Rev. Mat. Res. 42 (2012) 399–434.
[77] M. Naffouti, R. Backofen, M. Salvalaglio, T. Bottein, M. Lodari, A. Voigt, et al., Complex dewetting scenarios of ultrathin silicon films for large-scale nanoarchitectures, Sci. Adv. 3 (2017) eaao147.
[78] M. Bollani, M. Salvalaglio, A. Benali, M. Bouabdellaoui, M. Naffouti, M. Lodari, et al., Templated dewetting of single-crystal sub-millimeter-long nanowires and on-chip silicon circuits, Nat. Commun. 10 (2019) 5632.